2016 IEEE/RSJ International Conference on Intelligent Robots and Systems (IROS)
Daejeon Convention Center
October 9-14, 2016, Daejeon, Korea

Virtual Fixture Assistance for Needle Passing and Knot Tying

†Zihan Chen, Anand Malpani, Preetham Chalasani, Anton Deguet,
S. Swaroop Vedula, Peter Kazanzides and Russell H. Taylor

***Abstract*— Suturing is a challenging and highly dexterous task in minimally invasive surgery, even with the assistance of robotic surgical systems. In this work, we propose a simple yet versatile impedance virtual fixture framework, which can be applied on the master manipulator in a tele-operated robotic surgical system. With this framework, we further develop two types of virtual fixtures that assist with the needle passing and knot tying sub-tasks in suturing. The paper also presents the results of a 14-participant user study for both needle passing and knot tying sub-tasks, showing that virtual fixture assistance for novice users increases the needle passing exit point accuracy, reduces the number of errors (suture slip) in knot tying, and simultaneously decreases the task completion time and overall operator workload.**

I. Introduction

Minimally invasive surgery (MIS) is beneficial to patients due to the smaller incisions and faster recovery times. However, surgeons face the challenge of a limited and constrained workspace with loss of direct visualization. The development of robot-assisted surgery via the da Vinci surgical system [1] has tackled these challenges by providing the surgeon with wristed instruments, augmented stereo vision and better ergonomics. Even then, the dexterous manipulation involved in suturing and knot tying is challenging [2], making them mentally demanding and time consuming tasks in MIS. As a result, these skills are an important component of the training program of Fundamentals of Laparoscopic Surgery [3] and similar robot-assisted surgery training programs.

Some researchers have attempted to automate part of this challenging task using learning by demonstration algorithms. Mayer et al. [4] used a supervised learning algorithm on recorded trajectories from an experienced surgeon and generated a semi-automated procedure that can be "played back" by the robot at a later time, thus allowing automatic task completion. Similarly, Schulman et al. [5] used a trajectory transfer algorithm by performing a non-rigid registration between a demonstration trajectory, generated by a human, and a test scenario. A slightly different approach is to define the task analytically. Jackson and Cavusoglu [6] split the suturing task into five steps: Needle Approach, Needle Bite, Needle Reorientation, Needle Regrasping and Needle Follow Through, providing a path planning algorithm for each step. In a subsequent paper, Chow et al. [7] presented a vision guided automatic knot tying system, where the robot automatically ties a knot at a user selected position.

†Z. Chen, A. Malpani, P. Chalasani, A. Deguet, S.S. Vedula, P. Kazanzides and R.H. Taylor are with the Department of Computer Science, Johns Hopkins University, Baltimore, MD, USA. Z. Chen can be reached at zihan.chen@jhu.edu.

Although the fully autonomous and semi-autonomous approaches are promising, they will continue to be a challenge for the foreseeable future due to technical difficulties and regulatory concerns. Specifically, the suturing task in these works has been oversimplified and will require additional work to transfer to a real surgical setting. We have taken a surgeon-in-the-loop approach, where "virtual fixtures (VFs)" (e.g., [8], [9], [10], [11]) are used to reduce uncertainty in motion, thereby improving operation accuracy and reducing mental stress on the surgeon.

Kapoor et al. [9] presented a constrained optimizer framework to define VFs for a suturing task (catering to the needle alignment sub-step and bite sub-step) with a cooperative robot. Their experimental evaluation was limited to comparing the deviation of the performed trajectory from the ideal path. Later, the authors [10] applied the framework to a knot positioning task (the last step of knot tying task), which requires a multi-robot cooperation. VFs were used to maintain certain spatial relationships between the two cooperative robots. In a follow-up paper, Xia et al. [11] extended this approach to a master/slave teleoperation robot (da Vinci Surgical Robot) with the same knot positioning task. However, the authors only presented an experimental protocol without any experimental data proving its effectiveness.

In this paper, we implemented and validated VFs to assist the user during the needle passing and knot tying sub-tasks on a teleoperated robotic system. In Section II, we present a new approach to define VFs in the task frame, along with an explanation of the needle passing and knot tying VFs. Section III describes the system implementation details and the validation experiment and user study. The outcomes of the study and a discussion of the experimental findings is provided in Section IV. Finally, we conclude the paper by laying out possible future research directions in Section V.

II. Virtual Fixtures

VFs are used to augment sensory information by constraining or guiding motion in order to improve performance of a surgeon in direct or remotely manipulated tasks. In this paper, we implement a couple of VFs on the master side manipulators to enhance the accuracy and efficiency of the surgeon performing a suturing task. The da Vinci surgical system is highly optimized to follow motions of the master manipulator. Thus, we chose to implement these fixtures on the master side of the robot. Constraining the surgeon's hand motion by master-side VFs does not alter the basic position-based telemanipulation control loop of the robot

978-1-5090-3761-2/16/$31.00 ©2016 IEEE

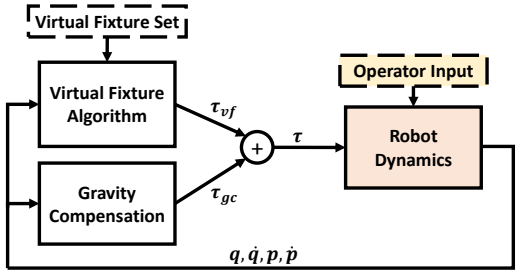

Fig. 1: Impedance Type Controller :
$\mathbf{q}$ - joint position; $\dot{\mathbf{q}}$ - joint velocity; $\mathbf{p}$ - Cartesian position; $\dot{\mathbf{p}}$ - Cartesian velocity; τ - total joint torque applied to robot; τ_{vf} - joint torque from virtual fixture controller; τ_{gc} - joint torque from gravity compensation.

and (therefore) does not interfere with the safety and system assurance associated with the basic telemanipulation function.

In the following subsections, we will discuss the implementations of the VF in detail – by describing the suturing task (Section II-A), by providing the generic formulation of an impedance type VF (II-B), and, by formulating the sub-task specific VF for the *needle passing* and *knot tying* steps (Sections II-C and II-D respectively).

A. Task Description and Analysis

Suturing is an important step across multiple surgical procedures and an integral component of surgical skills training curricula. It is also considered difficult to master in terms of dexterity and time consuming tasks in MIS [12]. Although specialized instruments like Endo Stitch™ (Covidien, Medtronic), are used in traditional MIS to reduce operating time, the conventional suturing and knot tying technique remains the most popular and cost effective method [13]. The suturing step often requires multiple attempts by the surgeon, which extends the operating time [12]. We believe that providing VF will increase the accuracy in task performance, and significantly decrease the time per stitch. This technique can be used to train novice surgeons.

B. Impedance Virtual Fixture

We have used impedance-type VF, wherein forces are exerted on the surgeon's hands to provide guidance. In our experience, these forces do not interfere significantly with basic control stability, and the slave manipulator simply follows the master motions. Furthermore, we can easily combine different assistance behaviors like gravity compensation with impedance VF by simply adding the desired joint torques that were computed for each case, as shown in Fig. 1.

To define the VF controller behavior, the teleoperation component sets a force/torque compliance frame $F_c = [R_c, \vec{p}_c]$ defined in the master base frame, together with position stiffness gains $\vec{k}^{(+)}, \vec{k}^{(-)}$, position damping gains $\vec{b}^{(+)}, \vec{b}^{(-)}$ and force bias terms $\vec{g}^{(+)}, \vec{g}^{(-)}$. Similarly, we have the orientation torque bias terms $\vec{\tau}^{(+)}, \vec{\tau}^{(-)}$ and orientation stiffness factors $\vec{k}_o^{(+)}, \vec{k}_o^{(-)}$. Desired forces and torques applied on the master tip are represented by $\vec{f}$ and $\vec{t}$, respectively. Given the current velocity $\dot{p}$, Algorithm 1 presents the pseudo-code for computing desired force and torque that should be applied on the master tip.

One advantage of our design for VF is that it permits very fast haptic rendering of discontinuous impedance environments in the local configuration space near the slave end effector, also allowing a very versatile description of local VF behavior. Further, it permits simple combinations of VF elements. Although the low-level VFs directly supported by this formulation are very simple, more complex VFs may be implemented by updating the parameters at a reasonably fast update rate that is nevertheless slower than the very fast rates associated with haptic rendering. In our current implementation, we use a haptic update rate of 1 KHz and a VF update rate of 500 Hz.

Algorithm 1 Impedance Virtual Fixture

if Enabled **then**
  # ——- Force ——-
  $\vec{q} = F_c^{-1}\vec{p} = R_c^{-1}(\vec{p} - \vec{p_c})$ ▷ Position Error
  $\vec{v} = R_c^{-1}\dot{p}$ ▷ Velocity on compliance frame
  for $i \in \{x, y, z\}$ **do**
    if $\vec{q}_i \leq 0$ **then**
      $\vec{g}_i = \vec{g}_i^{(-)} + \vec{k}_i^{(-)}\vec{q}_i + \vec{b}_i^{(-)}\vec{v}_i$
    else
      $\vec{g}_i = \vec{g}_i^{(+)} + \vec{k}_i^{(+)}\vec{q}_i + \vec{b}_i^{(+)}\vec{v}_i$
    end if
  end for
  $\vec{f} = R_c\vec{g}$ ▷ Desired force

  # ——- Torque ——-
  $\triangle R = R_c^{-1}R$
  Compute $\vec{\theta}$ such that $exp(skew(\vec{\theta})) = \triangle R$
  for $i \in \{x, y, z\}$ **do**
    if $\vec{\theta}_i \leq 0$ **then**
      $\vec{\tau}_i = \vec{\tau}_i^{(-)} + \vec{k}_{oi}^{(-)}\vec{\theta}_i$
    else
      $\vec{\tau}_i = \vec{\tau}_i^{(+)} + \vec{k}_{oi}^{(+)}\vec{\theta}_i$
    end if
  end for
  $\vec{t} = R_c\vec{\tau}$ ▷ Desired torque
end if

An example of a one-sided forbidden region plane virtual fixture is shown in Fig. 2. A 3D plane can be defined by a

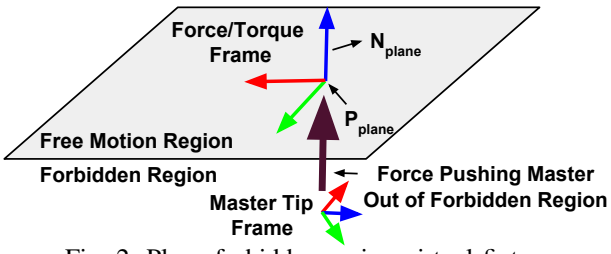

Fig. 2: Plane forbidden region virtual fixture

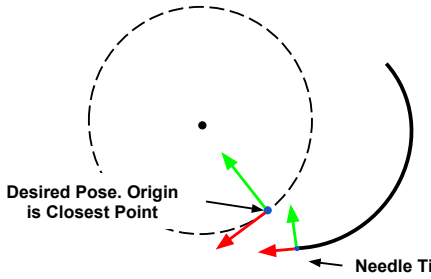

Fig. 3: Needle passing circular motion virtual fixture.

point p_{plane} and a vector N_{plane}, normal to the plane. The force/torque frame is defined with its origin at p_{plane} and its Z axis as N_{plane}. The X and Y axes can be chosen freely as long as they form a right-handed coordinate frame. For example, if the positive and negative force stiffness gains are set to $[0, 0, 0]$ and $[0, 0, 500]$ respectively, the user is free to move on one side of the plane while feeling a force pushing him/her away from the forbidden side of the plane.

C. Needle Passing Virtual Fixture

In the needle passing sub-task, we provide a three phase VF: (i) to bring the needle to a desired orientation, (ii) to guide the user to the entry point, and (iii) to guide the user to pierce through the tissue in a constrained circular motion. As the desired rotation and position are known to the system, transitions between the three VF phases are automatic based on rotation and position errors without any additional user interaction via a foot pedal, for example.

In this study, we used a 3D-printed needle holder (Fig. 7) to ensure that the needle was held consistently in a known relative pose across a user's trials (task repetitions). This allows us to factor out the effect of variability in the environment on the task performance and focus our analysis on evaluating design and effectiveness of the VF. The needle tip frame can be computed using robot forward kinematics and the known needle holder design. Computer vision techniques can be used to determine the relative pose of the needle with with reference to the robot tool tip frame, however, that would be out of the scope of this paper.

The user starts the VF by pressing the `CAMERA` pedal. Once the foot pedal event is detected, a force/torque compliance frame is defined at the current gripper position with a precomputed orientation based on the ideal entry pose for the needle. Positive gain values with zero offset are set for all three axes for the force and torque frames. This VF will apply a force and torque on the master manipulator to guide the user to orient the needle. The system constantly monitors the orientation error and moves on to the second phase if the error is within a set threshold value – determined empirically to ensure accuracy but at the same time allow smooth phase transition. In the second phase, the position of the force/torque compliance frame is changed to the desired position, while orientation and gain values remain unchanged.

After the needle is in the correct pose, the third phase VF is enabled to guide the user to pierce through the tissue. We define a circle with its origin at the center of the needle and the radius same as the needle radius to constrain the needle driving motion. The VF frame is updated every single loop by setting the origin as the closest point on the desired circle (see Fig. 3), the Y axis points towards the center of the circle, and the Z axis is normal to the plane of the circle. The VF position gains along the Y and Z axes are set to large values to maintain the needle along the circle, while the X axis gain is set to zero to allow the user to freely move along the needle and the circle. Orientation gains are set to large values for the three axes, enforcing the needle tip to move along the predefined circular path. The gain values were determined empirically – strong enough to provide effective guidance, but soft enough so that the user can over-power it when necessary to compensate for small modeling errors.

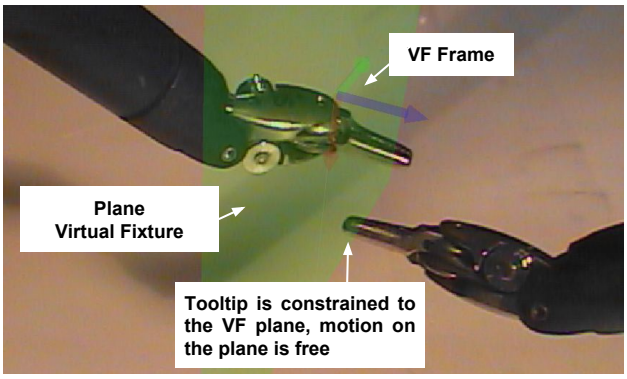

Fig. 4: Knot tying virtual fixture: a constraining plane (green) with its force/torque VF frame. It is showed here for demonstration purpose. Users can feel it haptically, but do not see the augmented plane visually.

D. Knot Tying

The surgeon's knot has three elements: a two loop knot followed by two single loop knots. Here we only focus on defining the VF for the two loop knot. A similar technique can easily be applied to the other single loop knots. One of the challenges faced by a novice user in knot tying is to successfully loop the thread twice around the instrument tip without slippage.

We use a plane VF (Fig. 4) to provide the novice user assistance during the looping action. The plane VF is located at the clevis point of the instrument in the non-dominant hand (the one on which the loop will be laid upon) with a normal along the instrument pointing direction. This is a constraining two-handed VF that allows the dominant instrument tip to move freely in the plane defined by the VF, and pulls it back towards the plane if there is any out of plane motion. A user can enable this VF by pressing and holding the `CAMERA MINUS` foot pedal. The VF gets activated only when the dominant instrument tip is close to the VF plane, in order to avoid a sudden large force from being applied to the user and resulting in an undesirable motion. The Z axis for the VF is aligned with the instrument pointing direction. The gain values are set to be large along +Z and -Z axis, and zero on the X and Y axes.

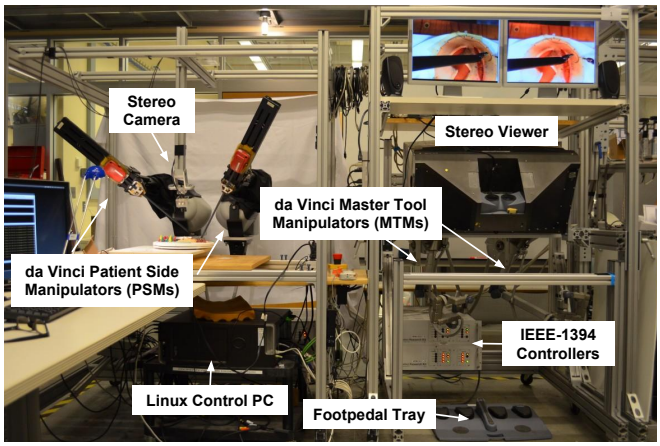

Fig. 5: da Vinci Research Kit experimental setup [14][15]

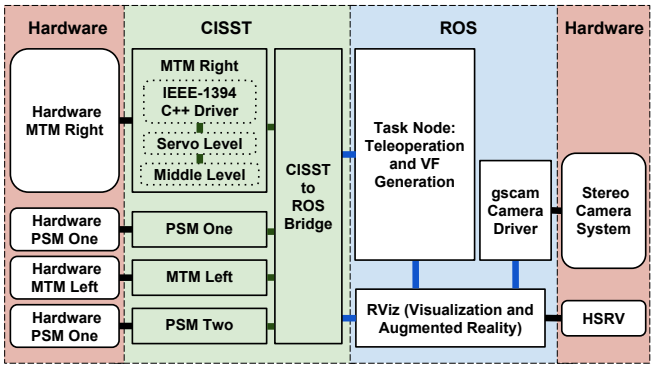

Fig. 6: Block diagram showing hardware/software connection, software components implemented in both *cisst* and ROS environments

III. Experiment

We conducted a user study to evaluate the effects of VF assistance in teleoperated robotic suturing sub-tasks *viz.* needle passing and knot tying. The implementation of the system architecture and the execution of the user study, along with the collected data and analyses are described in detail in the following sections.

A. System Implementation on da Vinci Research Kit

We have implemented the described VF framework on the da Vinci Research Kit (dVRK) platform [14][15], which is based on the first-generation da Vinci surgical system and shown in Fig. 5.

1) Hardware: The mechanical system of the dVRK (Fig. 5) consists of components from a dVSS Standard version robot – two 7 degrees-of-freedom (DOF) Master Tool Manipulators (MTMs), two 6-DOF Patient Side Manipulators (PSMs), a Foot Pedal Tray, and a High Resolution Stereo Viewer (upgraded to two flat panel displays configured to 1024 x 768 resolution, as compared to the standard dVRK systems that use CRT displays with 640 x 480 resolution). The different pedals on the foot tray can be pressed by the operators to trigger different events that change the control system states.

Each manipulator arm requires one controller box with two sets of custom electronics boards: (1) an IEEE-1394 FPGA control board, and (2) a Quad Linear Amplifier (QLA) board. All the controllers are daisy chained together on an IEEE-1394 (FireWire) bus and finally connected to a Linux control PC, enabling a centralized computation and distributed I/O architecture. The QLA board is a motor amplifier board, capable of supporting up to 4 axes and an output linear current of 6A. The FPGA board, mated on the QLA board, directly sends sensor feedback to the control PC and receives motor torque commands from the control PC. All controllers, including the lowest-level joint control, are implemented on the control PC. The controller interfaces with the robot manipulator through a DL-156 Zero Insertion Force connector.

Our stereo vision system comprises of two SONY lipstick cameras (see Fig. 5), which are connected to the dVRK stereo viewer console. A stereo camera calibration procedure is performed to obtain the intrinsic/extrinsic parameters for the camera that are later used for image rectification and camera registration. We note that although the stereo baseline and lens-to-tissue distances may be different if a regular da Vinci stereo camera is used, the stereo visualization provided is similar enough to allow us to evaluate our VF strategy.

2) Software: Within our centralized computation and distributed I/O architecture, all computation including I/O read/write, joint level 1kHz servo loop control and middle level robot state control (e.g., kinematics) are implemented on a Linux control PC. The lowest-level driver comprises a C++ API using the *libraw1394* library for IEEE-1394 communication. A component-based control architecture using the open-source cisst-SAW [16] libraries was implemented for the middle to high level robot control algorithms. Further, a *cisst* to Robot Operating System (ROS) bridge *cisst* component is added for interfacing the robots with other task level control logic, visualization and augmented reality software in a ROS-based environment. The system provides both joint level and Cartesian level API interfaces as well as functions to enable, disable and set impedance VFs on the master side manipulators.

Fig. 6 gives an overview of the software system, its connection to hardware and different components implemented in the *cisst* and ROS environment. The *Task Node* contains the task specific logic that defines and publishes virtual fixture commands to the masters based on task state. The *RViz* node is a ROS visualization software for visualizing robot configuration, displaying the live stereo video stream (grabbed with the *gscam* package) and adding augmented reality markers for visual guidance.

B. Test Setup

1) Needle Passing Sub-task: As shown in Fig. 7, a 15 mm thick tissue phantom is used in the experiment. This phantom has a stiff top layer simulating the epidermis and a soft dense foam layer simulating the dermis. A large needle driver instrument from Intuitive Surgical Inc. is chosen to operate a 3/8 circle 26 mm reverse cutting suture needle fixed in a 3D printed needle holder. The needle holder is designed

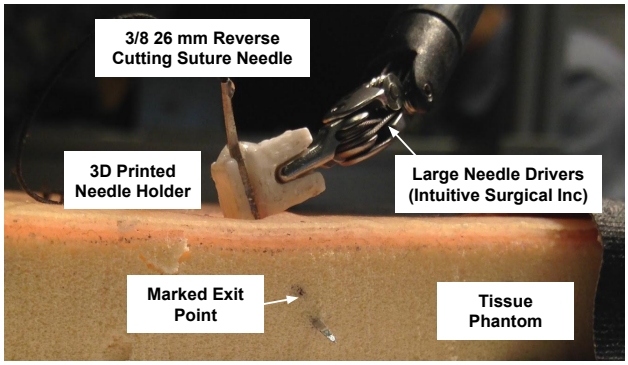

Fig. 7: Test setup for needle passing task, including tissue phantom, suturing needle with needle holder and a large needle driver instrument

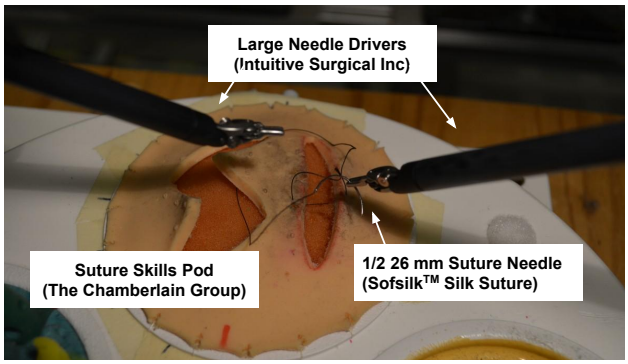

Fig. 8: Test setup including a suture skills pod (phantom), a suture needle and two large needle driver instruments

to tightly fit the large needle driver gripper to ensure that the needle cannot move with reference to the instrument during the test. On the tissue phantom, the target entry and exit points are marked with dark color dots such that they can be easily identified through the stereo viewer on the master console. The operating area is placed at the center of the camera view. Before each trial, the instrument is moved to the same starting pose.

2) Knot Tying Sub-task: Similar to the needle driving task, two large needle driver instruments (Intuitive Surgical Inc.) are installed on the patient side manipulators. Users teleoperate, with position scale of 0.3, the two instruments from the master console with visual feedback through the stereo viewer. Before the task, a suture thread of 18 cm total length was prepared on a suture skills training pod (The Chamberlain Group Inc.) commonly used for robotic surgery training. As shown in Fig. 8, the suture has a 3 cm tail left on the right side of the tissue for easy grasping, 2 cm between the entry and exit points on the phantom, and a 13 cm loose end for the knot tying operation. Again, all the robot arms are configured to the same starting poses.

C. Test Procedure

The user study was performed with volunteer users recruited from a population of graduate and undergraduate students at the Johns Hopkins University (JHU) and with none to little experience in teleoperated robotic suturing. Tests were approved by the JHU Homewood Institutional Review Board (HIRB00002925). A total of 14 participants, 13 right-handed and 1 ambidextrous, completed the trials (12 male, 2 female). None of the volunteers have neurological disorders, or uncorrected vision problems that may negatively affect performance.

The experiment was divided into four parts: an introduction section, needle passing sub-task section, knot tying sub-task section and the subjective evaluation section. Users started the experiment with an introduction to the suturing task by watching a video of simulated surgical suturing using the *da Vinci* skills simulator and brief introduction with hands on time to get familiar with basic da Vinci operation like teleoperation and clutch pedal. Before each sub-task, users were given sub-task specific instructions and guidance on how to use the sub-task specific VF before the trials. The subjects then practiced two non-recorded trials, with one in each control mode (freehand and VF assisted), to understand the system and the sub-task. After this, users practiced 4 consecutive trials in each control mode. The order in which the test conditions were practiced was balanced and randomized between users to cancel the learning effect. Users took a break between the two sub-tasks. Users completed a NASA TLX survey [17] after each sub-task and a subjective evaluation questionnaire at the end of the entire trial. The whole experiment lasted about 1.5 hours per user. None of the users verbalized fatigue as corroborated by the self-reported TLX survey.

D. Data Collection and Analysis

The states of the MTM and PSM robots (500 Hz), video stream (30 Hz) of the stereo cameras and foot pedals events were logged for all trials. For the needle passing task, exit points were also recorded with high-definition cameras, from where the exit error was measured. The performance of the needle passing task was evaluated in terms of exit error and task completion time. For the knot tying task, task completion time, total needle trajectory and times the suture slipped during the loop were used as performance evaluation metrics. For subjective evaluation, the standard NASA TLX survey is adopted to evaluate operator workload and the subjective evaluation questionnaire covers perceived difficulties during the suturing task, user preference on control mode and suggestions on how to improve robotic assistance.

IV. Results and Discussion

This section reports the results of the user study, including both sub-tasks. Each user completed multiple trials for each test condition, so a two-way repeated measure analysis of variance (ANOVA) is performed, where the test mode (freehand and VF-assisted) is the first independent variable and the user is treated as a random variable. For TLX workload analysis, a paired t-test is used.

A. Needle Passing Sub-task

1) Statistical Analysis: We analyzed total task completion time from the start of needle motion until the needle tip

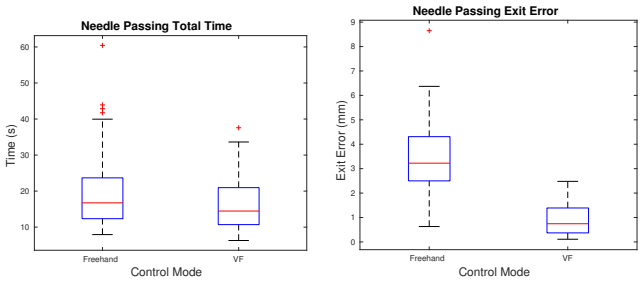

Fig. 9: Boxplots showing the needle passing task completion time under two test conditions (left) and needle exit point error (right). For all boxplots in this paper, the red centerline represents the median, the upper and lower edge of each box corresponds to 25th and 75th percentiles, and the whiskers extend to the most extreme data points. The red cross points are considered outliers [18].

pierces through tissue. Fig. 9(a) shows a boxplot of the total task completion time. The overall mean total task completion time was 18.17 seconds. The introduction of VF assistance reduced the mean task completion time by 15% from 19.67 s to 16.67 s. There was a significant effect of VF assistance ($F_{1,84} = 5.62$, $p = 0.02$) and user ($F_{13,84} = 6.33$, $p < 0.01$) on total task completion time. The interaction effect between VF assistance and user was also significant ($F_{13,84} = 3.23$, $p < 0.01$).

The measured exit error is defined as the distance between the marked target point and the needle exit point. Fig. 9(b) shows a boxplot of the measured exit error. The mean exit error when VF assistance is enabled was 3.38 mm, while the mean error in freehand mode was 0.88 mm. The effect was significant ($F_{1,84} = 155.36$, $p < 0.01$). The effect of users was also significant ($F_{13,84} = 2.63$, $p < 0.01$), but there was no significant interaction effect ($F_{13,84} = 1.05$, $p = 0.41$).

2) Trajectory Analysis: In comparing freehand to VF modes, we noticed that in freehand mode, users tend to first move down in a straight line with the intent to pierce the needle through the tissue before they even start rotating the needle. Fig. 10(a) illustrates this tendency. With VF assistance, the user moves and rotates the master simultaneously, resulting in a smooth circular motion as shown in Fig. 10(b), which can effectively reduce stress on the tissue.

Another important finding is that, in freehand mode, users tend to re-adjust the needle trajectory when they find that the needle exit point might be far away (e.g., 5 mm) from the target exit point by pulling the needle out vertically and redoing the operation, which could potentially increase the possibility of tearing tissues and explain the longer total task completion time.

3) Operator Workload: The boxplot shown in Fig. 11(a) summarizes the overall workload (the sum of the responses to all categories). The mean workload for freehand mode was 23.86 compared with 13.57 for VF assistance (the scale ranges from 6 to 42) and a paired t-test reveals that the effect of VF assistance is significant (p = 0.0005).

The radar plot in Fig. 12 shows the mean values of each

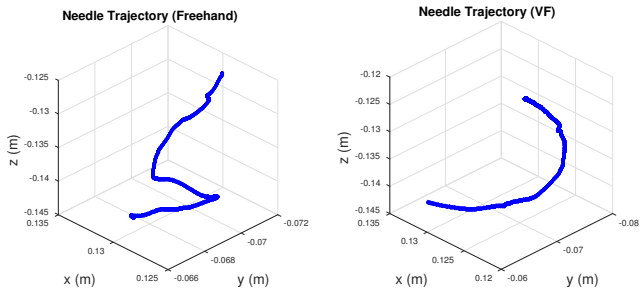

(a) Freehand (b) Virtual fixture assisted

Fig. 10: Comparison of needle passing trajectories: left is needle trajectory in freehand motion, right is trajectory from the same user with virtual fixture assistance.

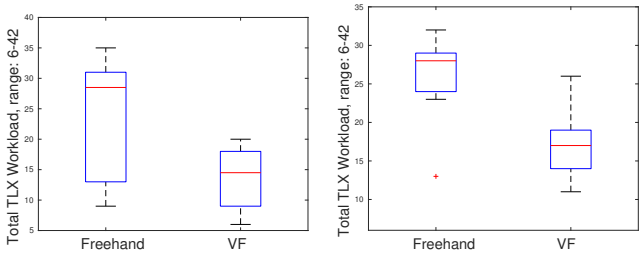

(a) Needle Passing (b) Knot Tying

Fig. 11: Boxplot showing the total operator workloads as self-reported via the NASA TLX survey for each test mode. Left is from the needle passing sub-task and right is from the knot tying sub-task.

workload category self-reported by the users in the NASA TLX survey. VF assisted needle passing resulted in less workload than the freehand mode in all categories.

4) Subjective Evaluation: Participants unanimously opted for VF-assisted mode rather than free-hand mode for the needle passing task. The ability to find the right entry orientation was the favorite feature. One user also suggested that a text hint on when to start and stop VF-assistance can be helpful.

B. Knot Tying Sub-task

1) Errors (Number of Slips): The motivation behind the plane VF is to prevent the slip events common for novice users. Our findings show that the plane VF does help reduce the average number of slips per trial from 1.5 in freehand mode to 0.34. The effect of VF assistance is significant ($F_{1,84} = 28.87$, $p < 0.01$). The data do not provide statistically significant evidence that the overall skill level of the "novice" participants was the same ($F_{13,84} = 1.47$, $p = 0.15$) or that the amount of improvement was uniform across users ($F_{13,84} = 1.17$, $p = 0.31$). Therefore, it is possible that the different users will benefit from VF assistance by different amounts. It needs to be pointed out that not all slips happened during the suture wrapping process. In fact, a few slips happened when the user had already finished the loop and was trying to reach and grab the suture tail, but failed due to lack of good depth perception

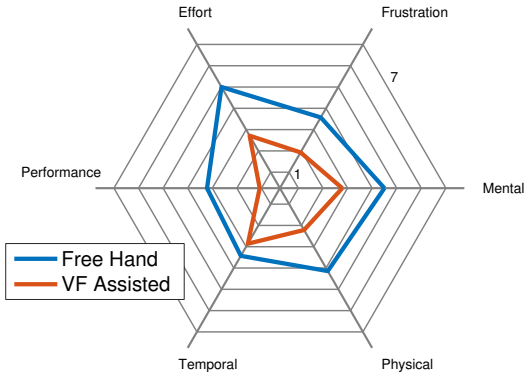

Fig. 12: Needle Passing Task, NASA TLX survey radar plot of average categorical workload as self-reported by the users. Workloads increase from the center.

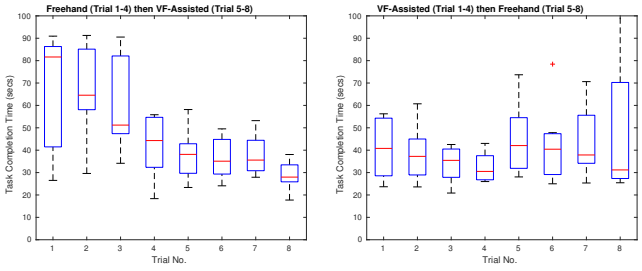

Fig. 13: Boxplots of knot tying task completion time versus trial number. The left figure is from users who did freehand mode first followed by VF-assisted mode and the right figure from users with the opposite order.

with the pair of small video cameras that we used. This issue can be alleviated by providing a better stereo visualization system.

2) Task completion and trajectory length: Noticeable benefits in task completion time were observed when using VF assistance ($F_{1,84} = 16.15$, $p < 0.01$). Similarly, a statistically significant difference in PSMs trajectory length (both of PSM1 and PSM2 trajectory) was also found ($F_{1,84} = 11.35$, $p < 0.01$ for PSM1, $F_{1,84} = 12.39$, $p < 0.01$ for PSM2). Fig. 13 shows boxplots of task completion time versus trial number from two different test orders. Users who did freehand mode first demonstrated a clear learning curve. Especially for the first trial, the mean completion time was 67.62 seconds for the freehand user compared with 49.71 seconds for the VF-assisted user. Although the difference is not statistically significant, it still suggests that VF-assistance can potentially help novice users complete the task in a more timely manner.

3) Operator Workload: A summary of the overall workload (the sum of the responses to all the categories in the TLX survey) is shown in Fig. 11(b). The overall mean operator workload is 26.57 for freehand mode and 16.93 for VF-assisted mode. The effect of assistance was significant (p = 0.0001054). Fig. 14 shows a radar plot of the mean ratings for each workload category. The radar plot shows that the VF assisted mode has a lower perceived workload in every one of the five categories. Also, compared with the needle passing

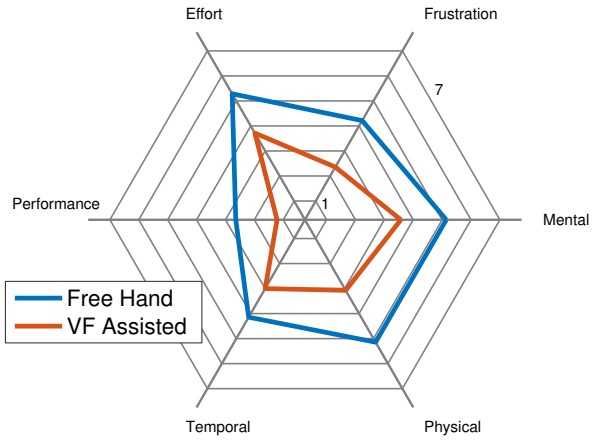

Fig. 14: Knot Tying Task, NASA TLX survey radar plot of average categorical workload as self-reported by the users. Workloads increase from the center.

sub-task, the knot tying task is a much more challenging task physically, mentally and requires more effort to finish.

4) Subjective Evaluation: In the questionnaire, 12 out of 14 users indicated that they prefer VF assistance to freehand mode. One of the two users who preferred freehand mode stated that the reason was that freehand mode felt less constrained. Another user suggested that giving a little more time to get used to the VF during the pre-evaluation phases of the experimental protocol might have improved performance.

V. Summary and Future Work

This paper has described the implementation of the virtual fixture assistance on a dVRK and reports the results of a user study to compare the performance of virtual fixture assistance and freehand teleoperation in both needle passing and knot tying suturing sub-tasks.

Despite bringing the benefits of small incisions and fast recovery times to the patient, MIS presents a constrained workspace and limited vision feedback for the surgeon. In particular, suturing remains the most demanding and time consuming task even with a teleoperated surgical system. This paper addresses these problems by providing impedance type VFs to assist the surgeon to complete the task in an accurate and efficient manner. These fixtures are applied on the master side without breaking the direct master to slave teleoperation link. In particular, a force compliance frame with force/torque gains and offsets is defined on the master workspace based on the current state of the task. This approach may have significant value in introducing VF assistance in complex telesurgical systems in which maintaining the integrity of a high bandwidth master-slave control loop is vital.

The results of our user study indicate that VF can significantly improve needle exit accuracy, thus reducing tissue tearing pressure. During the knot tying task, VF assistance reduces average task completing time, total trajectory length and number of slips during the task.

One interesting aspect of knot tying is that it is an inherently *two-handed* task. Accordingly, we developed a two-handed

VF to prevent the thread from slipping off the gripper during both the thread wrapping and tail grasping phases of tying the knot. The success of this strategy illustrates the potential importance of such two-handed, coordinated VFs in such tasks, and we plan to investigate these further for other tasks.

In other future work, we plan to develop and evaluate different approaches for knot tying VF. In this regard, we plan to explore the trade-offs involved in different VF implementations and gains for these tasks. Similarly, we recognize that computer vision techniques can be employed for needle tracking and improving augmented reality performance. Another area of future work is incorporating computer vision methods into our system to identify needle, thread, and tissue locations to help generate the VF constraints. Here, we will also use the stereo endoscopic camera available with the "classic" da Vinci system in our laboratory, which runs the same open-source software environment. We also plan to investigate the use of the third slave manipulator on the da Vinci system to assist the surgeon by e.g. assisting with tissue alignment for needle passing or by grabbing the thread end and feeding it to surgeon during knot tying.

ACKNOWLEDGMENTS

This work was supported in part by National Science Foundation NRI grants 1208540 and 1327657 and in part by JHU internal funds. S. Swaroop Vedula is partly supported by a grant from NIDCR R01DE025265-01. We gratefully acknowledge the assistance of Jonathan Bohren in software development.

REFERENCES

[1] "Intuitive surgical, inc." http://www.intuitivesurgical.com, accessed: 2015-02-26.

[2] H. Kang and J. T. Wen, "Robotic knot tying in minimally invasive surgeries," in *Intelligent Robots and Systems, 2002. IEEE/RSJ International Conference on*, vol. 2. IEEE, 2002, pp. 1421–1426.

[3] J. H. Peters, G. M. Fried, L. L. Swanstrom, N. J. Soper, L. F. Sillin, B. Schirmer, K. Hoffman, S. F. Committee *et al.*, "Development and validation of a comprehensive program of education and assessment of the basic fundamentals of laparoscopic surgery," *Surgery*, vol. 135, no. 1, pp. 21–27, 2004.

[4] H. Mayer, F. Gomez, D. Wierstra, I. Nagy, A. Knoll, and J. Schmidhuber, "A system for robotic heart surgery that learns to tie knots using recurrent neural networks," *Advanced Robotics*, vol. 22, no. 13-14, pp. 1521–1537, 2008.

[5] J. Schulman, A. Gupta, S. Venkatesan, M. Tayson-Frederick, and P. Abbeel, "A case study of trajectory transfer through non-rigid registration for a simplified suturing scenario," in *Intelligent Robots and Systems (IROS), 2013 IEEE/RSJ International Conference on*. IEEE, 2013, pp. 4111–4117.

[6] R. C. Jackson and M. C. Cavusoglu, "Needle path planning for autonomous robotic surgical suturing," in *Robotics and Automation (ICRA), 2013 IEEE International Conference on*. IEEE, 2013, pp. 1669–1675.

[7] D.-L. Chow, R. Jackson, M. Cavusoglu, and W. Newman, "A novel vision guided knot-tying method for autonomous robotic surgery," in *Automation Science and Engineering (CASE), 2014 IEEE International Conference on*, Aug 2014, pp. 504–508.

[8] L. B. Rosenberg, "Virtual fixtures: Perceptual tools for telerobotic manipulation," in *Virtual Reality Annual International Symposium, 1993., 1993 IEEE*. IEEE, 1993, pp. 76–82.

[9] A. Kapoor, M. Li, and R. H. Taylor, "Spatial motion constraints for robot assisted suturing using virtual fixtures," in *Medical Image Computing and Computer-Assisted Intervention–MICCAI 2005*. Springer, 2005, pp. 89–96.

[10] A. Kapoor and R. H. Taylor, "A constrained optimization approach to virtual fixtures for multi-handed tasks," in *Robotics and Automation (ICRA), 2008 IEEE International Conference on*. IEEE, 2008, pp. 3401–3406.

[11] T. Xia, A. Kapoor, P. Kazanzides, and R. Taylor, "A constrained optimization approach to virtual fixtures for multi-robot collaborative teleoperation," in *Intelligent Robots and Systems (IROS), 2011 IEEE/RSJ International Conference on*. IEEE, 2011, pp. 639–644.

[12] J. Ruurda, I. Broeders, B. Pulles, F. Kappelhof, and C. Van der Werken, "Manual robot assisted endoscopic suturing: time-action analysis in an experimental model," *Surgical endoscopy and other interventional techniques*, vol. 18, no. 8, pp. 1249–1252, 2004.

[13] N. T. Nguyen, K. L. Mayer, R. J. Bold, M. Larson, S. Foster, H. S. Ho, and B. M. Wolfe, "Laparoscopic suturing evaluation among surgical residents," *Journal of Surgical Research*, vol. 93, no. 1, pp. 133–136, 2000.

[14] Z. Chen, A. Deguet, R. Taylor, S. DiMaio, G. Fischer, and P. Kazanzides, "An open-source hardware and software platform for telesurgical robotics research," in *Proceedings of the MICCAI Workshop on Systems and Architecture for Computer Assisted Interventions, Nagoya, Japan*, 2013, pp. 22–26.

[15] P. Kazanzides, Z. Chen, A. Deguet, G. S. Fischer, R. H. Taylor, and S. P. DiMaio, "An open-source research kit for the da vinci® surgical system," in *Robotics and Automation (ICRA), 2014 IEEE International Conference on*. IEEE, 2014, pp. 6434–6439.

[16] A. Deguet, R. Kumar, R. Taylor, and P. Kazanzides, "The *cisst* libraries for computer assisted intervention systems," in *MICCAI Workshop on Systems and Arch. for Computer Assisted Interventions*, Midas Journal: http://hdl.handle.net/10380/1465, Sep 2008.

[17] S. G. Hart, "NASA-task load index (nasa-tlx); 20 years later," in *Proceedings of the human factors and ergonomics society annual meeting*, vol. 50, no. 9. Sage Publications, 2006, pp. 904–908.

[18] M. Frigge, D. C. Hoaglin, and B. Iglewicz, "Some implementations of the boxplot," *The American Statistician*, vol. 43, no. 1, pp. 50–54, 1989.